Photoproduction of nitric oxide in seawater

Ye Tian[1,2,3], Gui–Peng Yang[1,2,3], Chun–Ying Liu[1,2,3], Pei–Feng Li[3], Hong–Tao Chen[1,2,3], Hermann W. Bange[4]

[1]Key Laboratory of Marine Chemistry Theory and Technology, Ministry of Education, Qingdao, 266100, China

[2]Laboratory for Marine Ecology and Environmental Science, Qingdao National Laboratory for Marine Science and Technology, Qingdao 266071, China

[3]College of Chemistry and Chemical Engineering, Ocean University of China, Qingdao, 266100, China

[4] GEOMAR Helmholtz–Zentrum für Ozeanforschung Kiel, Kiel, 24105, Germany

Correspondence to: Chun–ying Liu (roseliu@ouc.edu.cn) and Hong–Tao Chen (chenht@ouc.edu.cn)

Abstract. Nitric oxide (NO) is a short–lived intermediate of the oceanic nitrogen cycle. However, our knowledge about its production and consumption pathways in oceanic environments is rudimentary. In order to decipher the major factors affecting NO photochemical production, we irradiated artificial seawater samples as well as 31 natural surface seawater samples in laboratory experiments. The seawater samples were collected during a cruise to the western tropical North Pacific Ocean (WTNP, a N/S section from 36 °to 2 °N along 146 °/143 °E with 6 and 12 stations, respectively, and a W/E section from 137 ° to 161 °E along the equator with 13 stations) from November 2015 to January 2016. NO photoproduction rates from dissolved nitrite in artificial seawater showed increasing trends with decreasing pH, increasing temperatures and increasing salinity. In contrast, NO photoproduction rates (average: $0.5 \pm 0.2 \times 10^{-12}$ mol L^{-1} s^{-1}) in the natural seawater samples from the WTNP did not show any correlations with pH, water temperature and salinity as well as dissolved inorganic nitrite concentrations. The flux induced by NO photoproduction in the WTNP (average: 13×10^{-12} mol m^{-2} s^{-1}) were significantly larger than the NO air–sea flux densities (average: 1.8×10^{-12} mol m^{-2} s^{-1}) indicating a further NO loss process in the surface layer.

1 Introduction

Nitric oxide (NO) is a short–lived intermediate of the oceanic nitrogen cycle, see e.g. Bange (2008) and Kuypers et al. (2018). There are only a few reports about oceanic NO determination method so far because of its reactivity (Zafiriou et al., 1980; Lutterbeck and Bange, 2015; Liu et al., 2017). NO is produced and consumed during various microbial processes such as nitrification, denitrification and

anammox (Schreiber et al., 2012; Kuypers et al., 2018). Moreover, it is known that both phytoplankton and zooplankton can metabolize NO and are influenced by ambient (extracellular) NO concentrations (Singh and Lal, 2016; Wang et al., 2017; Astier et al., 2018).

Apart from (micro)biological processes, NO can be produced photochemically from dissolved nitrite (NO_2^-) in the sunlit surface ocean (Zafiriou and True, 1979; Zafiriou and McFarland, 1981):

$$NO_2^- + H_2O \xrightarrow{h\nu} NO + OH + OH^- \quad \text{(R 1)}$$

Mack and Bolton (1999) had reviewed the possible subsequent reaction like the produced NO and hydroxyl radical (OH) could react to produce HNO_2 reversely (R2), and some reaction that consumed NO like R3 to R7

$$NO + OH \rightarrow HNO_2 \quad \text{(R 2)}$$

$$NO + NO_2 \rightarrow N_2O_3 \quad \text{(R 3)}$$

$$N_2O_3 + H_2O \rightarrow 2H^+ + 2NO_2^- \quad \text{(R 3)}$$

$$NO + NO \rightarrow N_2O_2 + O_2 \rightarrow N_2O_4 \quad \text{(R 4)}$$

$$2NO_2 \rightarrow N_2O_4 \quad \text{(R 5)}$$

$$N_2O_4 + H_2O \rightarrow 2H^+ + NO_2^- + NO_3^- \quad \text{(R 6)}$$

besides, in natural sunlit seawater, photolyzed dissolved nitrate (NO_3^-) could be a potential source of NO through NO_2^- (R 8); during the process of ammonium (NH_4^+/NH_3) oxidation into NO_2^- and NO_3^-, NO might be an intermedium (Joussotdubien and Kadiri, 1970), or NO could be produced through amino–peroxyl radicals ($NH_2O_2^\cdot$) through R 8 to R 11 (Laszlo et al., 1998;Clarke et al., 2008)

$$NO_3^- \xrightarrow{h\nu} NO_2^- + \frac{1}{2}O_2 \quad \text{(R 7)}$$

$$OH^\cdot + HCO_3^-/CO_3^{2-} \rightarrow CO_3^{\cdot-} + H_2O/OH^- \quad \text{(R 8)}$$

$$OH^\cdot + NH_3 \rightarrow NH_2^\cdot + H_2O \quad \text{(R 9)}$$

$$CO_3^{\cdot-} + NH_3 \rightarrow NH_2^\cdot + HCO_3^- \quad \text{(R 10)}$$

$$NH_2^\cdot + O_2 \rightarrow NH_2O_2^\cdot \quad \text{(R 11)}$$

$$NH_2O_2^\cdot \rightarrow NO^\cdot + H_2O \quad \text{(R 12)}$$

Table 1 summarized studies about photochemical production of NO measured in the surface waters of the equatorial Pacific Ocean (Zafiriou et al., 1980; Zafiriou and McFarland, 1981), the Seto Inland Sea (Olasehinde et al., 2009; Olasehinde et al., 2010; Anifowose and Sakugawa, 2017), the Bohai and Yellow Seas(Liu et al., 2017; Tian et al., 2018) and the Kurose River (Japan) (Olasehinde et al., 2009; Anifowose

et al., 2015). NO photoproduction rates varied among different seawater samples, it seemed the rates in Kurose River (average: 499 $\times 10^{-12}$ mol L^{-1} s^{-1}) was biggest, which was possibly due to an increase of nitrite being released into the river in agricultural activity during the study time. However, NO concentration was about 1.6 $\times 10^{-12}$ mol L^{-1}, at lowest level, which was because of higher scavenging rate in river water (NO lifetime :0.25 s). The lifetime of NO showed increasing trend from river (several seconds) to inland sea (dozens of seconds) to open sea (dozens to hundreds of seconds), reviewed in Anifowose and Sakugawa (2017). However, NO showed higher concentration level in coastal waters than in open sea, higher photoproduction rates might account for this.

In this study, we present the results of our measurements of NO photoproduction in laboratory experiments using artificial and natural seawater samples. The major objectives of our studies were (i) to decipher the factors affecting NO photoproduction in seawater, (ii) to determine the photoproduction rates of NO from samples collected during a cruise to the western tropical North Pacific Ocean (WTNP) and (iii) to quantify the role of photoproduction as a source of NO in the surface waters of the WTNP.

2 Methods

2.1 Determination of dissolved NO in aqueous samples

For the measurements of dissolved NO we applied the method described by Olasehinde et al. (2009): In brief, NO in the aqueous samples was determined by trapping it with added 4,5–diaminofluorescein (DAF–2, chromatographic grade from Sigma–Aldrich, USA) and measuring the reaction product triazolofluorescein (DAF–2T) with a high performance liquid chromatography system (HPLC). We used an Agilent 1260 Infinity HPLC (Agilent Technologies Inc., USA) system equipped with a Venusil XBP–C18 column (5.0 µm; 4.6 mm × 250 mm i.d.). The column temperature was set to 25°C and the mobile phase was comprised of acetonitrile (HPLC grade from Merck, Darmstadt, Germany) and phosphate buffer (disodium hydrogen phosphate heptahydrate, guaranteed reagent from Sinopharm Chemical Reagent Co., Ltd, Shanghai, China) solution (10 mmol L^{-1} at pH 7.4) with a ratio of 8:92 (*v*:*v*) and a flow rate of 1 mL min^{-1} in the isocratic mode.

The injected sample volume was 5.0 µL. The eluate was analyzed with a fluorescence diode array detector at wavelengths of 495 and 515 nm for excitation and emission, respectively. The retention time of DAF–2T was about 5.5 min.

An aliquot of 10 mL artificial seawater was bubbled with N_2 gas at a flow of 10 mL min^{-1} for 2 h to remove O_2 after 10 min of ultrasonic and heat degassing. The solution was then bubbled with high-purity NO gas (99.9 %, Dalian Date Gas Ltd., China) for 30 min. The concentration of the saturated NO stock solution was 1.4 mmol L^{-1}, which could be used within 3 h (Lantoine et al., 1995). A series of diluted NO solutions were prepared in N_2-purged water from the NO stock solution using a microsyringe (Xing et al., 2005; Liu et al., 2017). And the series samples were trapped by DAF-2 solution.

The detection limit of dissolved NO in Milli–Q water was 9.0×10^{-11} mol L^{-1}, which was determined by S/N=3 (3×0.03) with the blank samples (n=7) and the slope (0.101) in the low concentration range (3.3 – 33×10^{-10} mol L^{-1}). And average relative standard error of the NO measurements was +/– 5.7 % at a concentration of 3.0×10^{-9} mol L^{-1}.

2.2 Set–up of irradiation experiments

We performed irradiation experiments with Milli–Q water (18.2 MΩ cm, Millipore Company, USA), artificial seawater and natural seawater samples. Artificial seawater was prepared by dissolving 23.96 g NaCl, 5.08 g $MgCl_2$, 3.99 g Na_2SO_4, 1.12 g $CaCl_2$, 0.67 g KCl, 0.20 g $NaHCO_3$, 0.10 g KBr, 0.03 g H_3BO_3 and 0.03 g NaF in 1 L of Milli–Q water (Bajt et al., 1997) and filtered by 0.2 μm polyethersulfone membrane (Pall, USA) before the experiments.

All irradiation experiments (except the experiments for the temperature dependence, see section below) were conducted at a constant temperature of 20 ℃ by controlling the temperature of thermostat water bath (LAUDA Dr. R. Wobser Gmbh & Co. KG, Germany). The height of cylindroid quartz cuvette used for irradiation was 70 mm and the inner diameter was 14 mm with the volume about 10 mL. The optical pathlength was about 70 mm. During the experiment, the quartz cuvette, filled with 10 mL sample and blocked by PTFE stopper, was installed in the simulator and a little higher than the water bath surface. All quartz cuvettes were treated in the same manner except the cuvettes wrapped in aluminum foil which served as dark control.

Milli–Q water and artificial seawater samples were spiked with varying amounts of $NaNO_2$ (puriss. p.a. ACS grade from Sigma–Aldrich, USA; for details see sections below). All other chemicals were of analytical grade from Tianjin Kemiou Chemical Reagent Co., Ltd or Shanghai Sinopharm Chemical Reagent Co., Ltd.

Triplicate samples from each treatment were collected every 0.5 h with an entire irradiation time of 2 h. At the sampling time, the SUNTEST CPS+ was turned off and triplicate subsamples were collected from each sample in dark with microsyringe (50 μL), and then the cuvettes were quickly put back into the water bath to continue the experiment until two hours.The data from the experiments with Milli–Q and artificial seawater samples were fitted with a simple linear regression in artificial seawater samples (see below). However, a linear relationship was not found > 30 min for the natural seawater samples, therefore, we decided to choose 30 min as the total experimental time for natural seawater samples. Statistical analyses were done using SPSS v.16.0 or Origin 9.0 and results were considered significant at $p \leq 0.05$. The artificial light source was a 1.5 kW xenon lamp, which provided a light intensity of 765 W m^{-2}. The lamp was installed in an immersion well photochemical reactor called SUNTEST CPS+ solar simulator produced by ATLAS, Germany. The solar simulator employed in this study has been demonstrated to produce spectra which mimics that of the solar radiation and emits a radiation of wavelength from 300 to 800 nm (Wu et al., 2015).

2.3 Experimental outline

2.3.1 Optimal DAF–2 concentration and storage time

In order to find out the optimal DAF–2 concentration, 10 mL of artificial seawater containing 0.5 μmol L^{-1} NO_2^- was irradiated with various concentrations of DAF–2 ranging from 0.7 μmol L^{-1} to 4.8 μmol L^{-1} for 2 h.

To ascertain the sample storage time, 10 mL with artificial seawater samples containing 5.0 μmol L^{-1} or 0.5 μmol L^{-1} NO_2^- were irradiated with various concentrations of DAF–2 for 2 h. After irradiation, samples were kept in the dark and measured every 2 h.

2.3.2 Influence of pH, temperature, salinity and wave lengths

The influence of the pH was assessed by adjusting artificial seawater samples to pH levels of 7.1, 7.6 and 8.1 by addition of appropriate amounts of hydrochloric acid (2 mol L^{-1}) or caustic soda solution (2 mol L^{-1}).

To assess the influence of the temperature, artificial seawater samples were adjusted to temperatures of 10 ℃, 20 ℃ and 30 ℃ by controlling the temperature of the thermostat water bath.

To assess the influence of the salinity on the photoproduction of NO from dissolved NO_2^-, artificial seawater samples were adjusted to different salinity of 20, 30 and 35 by adding Milli–Q water or NaCl to the stock solution of artificial seawater.

In order to compare the contributions of ultraviolet A (UVA), ultraviolet B (UVB) and visible light to the NO photoproduction, two kinds of light filter film were used (wrapped around the quartz cuvette tubes: (i) a Mylar plastic film (from United States Plastic Cor., Lima, Ohio) which can only shield UVB and (ii) a film, always used as car insulation film (from CPFilm Inc., USA) shielding both UVA and UVB (Li et al., 2010;Wu et al., 2015).

2.4 Calculations of photoproduction rates (R_{NO}), photoproduction rate constant (J_{NO}) and reaction yield

For the artificial seawater experiments determining the generation of NO from the NO_2^- photochemical degradation, the data fitted with a simple linear regression with the form $y = R_{NO} \times t + b$, where y is the NO concentration which was calculated by the signal intensity of DAF–2T at time t and R_{NO} is the photoproduction rate.

The photoproduction rate constant of NO from nitrite (J_{NO}) was determined by preparing different concentrations of NO_2^- (0.5, 2.0 and 5.0 μmol L^{-1}) in Milli–Q water and artificial seawater. The slope of the linear correlation between photoproduction rates and concentrations of NO_2^- represents J_{NO} (Anifowose et al., 2015).

The yield of NO formation ($\%f_{NO}$) from the photodegradation via NO_2^- was estimated according to Anifowose et al. (2015)

$$\%f_{NO} = 100 \times J_{NO} \times c(NO_2^-) \times R_{NO}^{-1} \quad \text{(Eq 1)}$$

where $c(NO_2^-)$ is the initial concentration of NO_2^-.

2.5 Seawater samples

Surface seawater samples were collected form a water depth of 1 m during a ship campaign to the western tropical North Pacific Ocean on board the R/V “Dong Fang Hong 2” from 13 November 2015 to 5 January 2016. This cruise covered two sections: a N/S section from 36 to 2 °N along 146/143 °E with 6 and 12 stations, respectively, and a W/E section from 137 to 161 °E along the equator with 13 stations (Fig. 1). Stations S0701 – S0723 were sampled between 11 and 28 November (i.e. the first part of the N/S section), followed by sampling of W/E section between 16 and 27 December and sampling of

stations S0725 – S0735 between 30 December 2015 and 05 January 2016 (i.e. second part of the N/S section). In addition, relevant surface currents are indicated in Fig. 1 (Fine et al., 1994; Zhao et al., 2016; Zhang et al., 2018). The location of the Kuroshio Current on 15 November 2015 was taken from https://www1.kaiho.mlit.go.jp/.

Seawater samples were collected using 8–liter Niskin bottles equipped with silicon O–rings and Teflon–coated springs and mounted on a Sea–Bird CTD (conductivity, temperature, depth) instrument (Sea–Bird Electronics, Inc., USA). A 750 mL black glass bottle was rinsed with in situ seawater three times, and then was filled with seawater quickly through a siphon. When the overflowed sample reached the half volume of the bottle, the siphon was withdrawn rapidly, and the bottle was sealed quickly. Samples were filtered through 0.45 μm and 0.2 μm polyethersulfone membranes (Pall, USA) to minimize microbial influence (Kieber et al., 1996; Yang et al., 2011). Then the filtered seawater was transferred in the dark into acid–cleaned and pre–combusted amber glass bottles, stored in darkness at 4 ℃ and brought back to the laboratory on land. Samples were re–filtered with 0.2 μm polyethersulfone membranes (Pall, USA) before the irradiation experiments. DAF–2 solutions were added in the dark. The irradiation experiments were conducted within two weeks after the samples arrived in the land laboratory, the maximum storage time was about two months.

2.6 Dissolved inorganic nitrogen (DIN) and pH measurements

The concentrations of dissolved inorganic nitrogen (DIN = nitrate, nitrite, and ammonium) from the cruise were analyzed using an automated nutrient analyzer (SKALAR San++ system, SKAlAR, Netherlands) onboard. The detection limits were 0.05 μmol L^{-1} for nitrate, nitrite and ammonium. When the concentration was below detection limit, $^1/_2$ of the detection limit (0.025 round-off to 0.02) was used.

The pH values were measured just before the experiments by using a benchtop pH meter (Orion Star A211, Thermo Scientific ™, USA) which was equipped with an Orion 8102 Ross combination pH electrode (Thermo Scientific ™, USA). In order to ensure comparability with the temperature in the irradiation experiments, pH values of the natural seawater samples were measured at 20 ℃. The pH meter was calibrated with three NIST–traceable pH buffers (pH = 4.01, 7.00 and 10.01 at 20 ℃). The precision of pH measurements was +/–0.01.

3 Results and Discussion

3.1 Optimal DAF–2 concentration and storage time

NO concentrations generated from photolysis of artificial seawater samples with an initial NO_2^- concentration of 0.5 µmol L^{-1} increased with increasing DAF–2 concentrations and reached a maximum at a DAF–2 concentration of 1.4 µmol L^{-1} (Fig. 2a). At DAF–2 concentrations >1.4 µmol L^{-1} no further increase of the NO concentrations was observed. Thus, we used a DAF–2 concentration of 1.4 µmol L^{-1} for all experiments.

Samples after reaction with DAF–2 and stored at 4 ℃ in the dark were stable for at least 28 h with the measurement interval about 2 h (Fig. 2b). The relative standard deviations of the resulting NO concentrations after irradiating samples containing 0.5 µmol L^{-1} and 5.0 µmol L^{-1} NO_2^- were +/– 13% and +/– 7%, respectively. This demonstrated that photolysis samples with NO which were allowed to react with DAF–2 could be stored for at least one day at 4 ℃ in the dark.

3.2 Photoproduction of NO in Milli–Q water and artificial seawater

The photoproduction rates of NO in samples with NO_2^- concentrations of 0.5, 2.0 and 5.0 µmol L^{-1} were generally higher in artificial seawater than in Milli–Q water (Fig. 3a and 3b).

The resulting J_{NO} were 5.6 $\pm$0.9 $\times 10^{-4}$ min^{-1} and 9.4 $\pm$1.4 $\times 10^{-4}$ min^{-1} for Milli–Q water and artificial seawater, respectively. They are lower than the J_{NO} of 34.2 $\times 10^{-4}$ min^{-1} for Milli–Q water reported by Anifowose et al. (2015). The difference might be explained by different experimental set–ups such as sample self–shading, in our study, the quartz cuvette was 70 mm height and inner diameter was 14 mm with the volume about 10 mL while in Anifowose et al. (2015), the quartz photochemical reaction cell was 3 cm in diameter, 1.5 cm in length, and had a 6.5 mL capacity.

3.3 Influence of pH, temperature, salinity and wavelengths

All irradiation experiments were conducted in artificial seawater with two different NO_2^- concentrations of 0.5 and 5.0 µmol L^{-1}. The resulting NO concentrations were generally higher when irradiating the samples with the initial NO_2^- concentration of 5.0 µmol L^{-1}. NO photoproduction rates showed increasing trends with decreasing pH, increasing temperatures and increasing salinity, the relationship between rates with salinity and temperature rates is significant ($p < 0.5$) (Fig. 4 and 5).

Reaction (1) indicates that decreasing pH which results in lower concentrations of OH^- which, in turn, will promote NO formation via NO_2^-. This is in line with the finding of Li et al. (2011) who found that the photodegradation rate of NO_2^- in Milli–Q water was higher at pH = 6.5 than at pH = 9.5. Tugaoen et al. (2018) also found the effect of lowering pH to conjugate NO_2^- to HONO allowed for HONO photolysis (pH = 2.5). Besides, higher pH could also inhibit N_2O_4 and N_2O_3 hydrolysis reaction (R4 and R7) as reviewed by Mack and Bolton (1999). However in previous study of Chu and Anastasio (2007) and Zellner et al. (1990), the quantum yield of OH (which equals to the quantum yield of NO) was constant at the pH ranges from 6.0 to 8.0 and 5.0 to 9.0 under single wavelength light in nitrite solution. This might indicated that decreasing pH in our study mainly reduced NO consumption rather than increased NO production.

Higher temperatures led to increasing NO photoproduction rates according to the temperature dependence of chemical reactions given by the Arrhenius formula:

$$R = A \times \exp\left(-\frac{E}{R \times T}\right) \quad \text{(Eq 2)}$$

where A is an Arrhenius prefactor and T is the temperature (K). This indicates that an increasing temperature results in a higher rate, Chu and Anastasio (2007) also found that quantum yield of OH (or NO) showed a decreasing trend from 295K, 263K to 240K. Moreover, this equation can be used to consider the difference of the rates at two temperatures $T1$ and $T2$:

$$R_{T2} = R_{T1} \times \exp\left(\frac{E}{R} \times \left(\frac{1}{T1} - \frac{1}{T2}\right)\right) \quad \text{(Eq 3)}$$

If we assumed that E was a constant in the temperature ranges of 10 to 30 ℃ when NO_2^- = 0.5 μmol L^{-1}, and we plot ln R against 1/T, we would get the E value as 57.5 kJ mol^{-1} K^{-1}. Using the photoproduction rate at 20 ℃ (293.15 K) as our reference point ($T1$), an expression of the R_T with the temperature was as follows:

$$R_T = 2.7 \times 10^{-10} \times \exp\left(6920 \times \left(\frac{1}{293.15} - \frac{1}{T2}\right)\right) \quad \text{(Eq 4)}$$

Similarly, we could conclude expression of the R_T with the temperature when NO_2^- = 5.0 μmol L^{-1},

$$R_T = 7 \times 10^{-10} \times \exp\left(11026 \times \left(\frac{1}{293.15} - \frac{1}{T2}\right)\right) \quad \text{(Eq 5).}$$

However, NO production rate at 0.5 μmol L^{-1} nitrite did not increase from 20 to 30 ℃, the plausible explanation was that NO_2^- concentration here was the mainly influencing factor, NO_2^- might be run out

253 at 20 ℃, if NO_2^- concentration increased, like up to 5.0 μmol L^{-1}, the temperature could make a noticeable
254 difference.
255 Higher salinity obviously enhanced photoproduction rates of NO in both Milli–Q water and artificial
256 seawater samples (with 0.5 μmol L^{-1} or 5.0 μmol L^{-1} initial NO_2^- concentrations). The regression
257 relationship is y = 0.37 x – 4.55 for 0.5 μmol L^{-1} NO_2^- and y=2.3 x – 39.5 for 5.0 μmol L^{-1} NO_2^-,
258 respectively, where x is the salinity (‰) and y is the photoproduction rate ($\times 10^{-10}$ mol L^{-1} s^{-1}). This result
259 indicates that with increasing ion strength NO production is enhanced, however, the exact mechanism is
260 unknown and need further study. Zafiriou and McFarland (1981) also demonstrated that artificial
261 seawater comprised with major and minor salts showed complex interactions. But Chu and Anastasio
262 (2007) reported that added Na_2SO_4 (4.0–7.0 mmol L^{-1}) in solution had no effect on the quantum yield of
263 OH.
264 The highest NO photoproduction rates were observed with full wave length band whereas the lowest NO
265 rates were observed with UVB. The NO photoproduction rates approached zero at wave lengths in the
266 visible band. The contribution of visible band, UVA band and UVB band were <1%, 30.7 %, 85.2 % and
267 <1.0 %, 34.2 %, 63.1 % for 0.5 and 5.0 μmol L^{-1} NO_2^-, respectively. Our results are in line with the
268 findings of Zafiriou and McFarland (1981) who found that samples exposed to (UV+visible) wave
269 lengths lost NO_2^- more rapidly than those exposed only to the visible wave lengths alone. Chu and
270 Anastasio (2007) found that under single wavelength light, quantum yield of OH decreased with the
271 wavelength (280 nm to 360 and plateau until 390) which meant that single wavelength light of UVB had
272 higher photoproduction rate than UVA. Since it might be because of the wild band of UVA (320–420
273 nm) that led to the summational higher rates under UVA than UVB (in our system 300-320). Moreover,
274 according to the UV–visible absorption spectra of NO_2^-, λ_{max} was 354 nm, which is in the range of UVA
275 (320–420 nm) (Zuo and Deng, 1998; Zafiriou and McFarland, 1981).

276 **3.4 Kinetics of the NO photoproduction**

277 The yields of NO formation from NO_2^- (%f_{NO}) in artificial seawater samples were about 70.1% and 97.9%
278 for the initial NO_2^- concentrations of 0.5 and 5.0 μmol L^{-1}, respectively. The missing NO yield (29.9%
279 for 0.5 μmol L^{-1} and 2.1% for 5.0 μmol L^{-1}) might result from NO production via other (unknown)
280 nitrogen–containing substrates (Anifowose et al., 2015). Another plausible explanation would be that
281 during the process of NO_2^- photoproduction, some NO were oxidized into NO_2, then NO_2 dimerized (R5)

and the dipolymer N_2O_4 would hydrolyze into NO_2^- and NO_3^- (R7), which actually reduce the concentration of NO_2^- (Mack and Bolton, 1999).

Assuming a 100% yield from NO_2^- degradation and a fast reaction of NO with DAF–2 the observed linear relationships during the various irradiation experiments (Fig. 6) indicate that NO photoproduction was following a pseudo zero–order reaction. However, the R_{NO} ratios (average: 4.8) listed in Table 2 were not the same for the experiments despite the fact that the ratio of the initial NO_2^- concentrations (= 10) was the same for all experiments. This result, however, does point to reaction which is different from a zero–order reaction.

3.5 Photoproduction rates of NO in the western tropical North Pacific Ocean

During the cruise surface temperatures and salinities were in the range from 22.15 ℃ to 30.19 ℃ and 34.57 to 35.05 respectively. The concentrations of NO_3^-, NH_4^+ and NO_2^- ranged from 0.03 μmol L^{-1} to 1.6 μmol L^{-1}, 0.20 μmol L^{-1} to 1.2 μmol L^{-1} and 0.02 μmol L^{-1} to 0.33 μmol L^{-1}, respectively (Fig. 6). The measured photoproduction rates of NO ranged from 0.3 $\times 10^{-10}$ mol L^{-1} min^{-1} (station S0711) to 2.9 $\times 10^{-10}$ mol L^{-1} min^{-1} (station S0303), with an average value of 13.0 ± 7.6 $\times 10^{-11}$ mol L^{-1} min^{-1}. Photoproduction rates did not show significant correlations with NO_2^-, NO_3^-, NH_4^+, pH, salinity, water temperature as well as with colored dissolved organic matter (data not shown, the same method with Zhu et al. (2017))(statistics computed with SPSS v.16.0).

The non–existing linear relationship between R_{NO} and dissolved NO_2^- during our cruise is in contrast to the results of Olasehinde et al. (2010), Anifowose et al. (2015) and Anifowose and Sakugawa (2017) who observed positive linear relationships between NO photoproduction rates and the NO_2^- concentrations in the surface waters of the Seto Inland Sea and the Kurose River. This might because that other factors like pH, salinity were different between samples collected at different stations.

In Table 1, we found that the average photoproduction rate of NO measured in our cruise is lower than that of the Seto Inland Sea and the Kurose River which could be ascribed to higher background NO_2^- in the inland sea waters (Olasehinde et al., 2009; 2010). Our result is slightly lower than the R_{NO} from the central equatorial Pacific Ocean (> 10^{-12} mol L^{-1} s^{-1}), the lower concentration of NO_2^- (0.06 μmol L^{-1}) in our study area might account for this (Zafiriou and McFarland, 1981). In Table 1, the NO_2^- concentration of 0.06 μmol L^{-1} in our study was lower than most of other study area like Qingdao coastal waters (0.75 μmol L^{-1}) and the Seto Inland Sea (0-0.4 μmol L^{-1} or 0.5-2 μmol L^{-1}). In the study of

311 Anifowose et al. (2015), since the NO_2^- concentration of upstream K1 station was similar to ours (0.06
312 μmol L^{-1}), the higher R_{NO} might attributed to lower pH (7.36) as mentioned above.Or it might be because
313 the difference of the river water and the seawater, considering lower nitrite level of K1, dissolved organic
314 matter might also account for the higher R_{NO}. Because of its conservative mixing behavior with salinity,
315 dissolved organic matter always showed higher level in river than open sea (Zhu et al., 2017), which
316 could photodegrade itself to produce NO_2^-, finally to promote R_{NO}. In our study, the rates were adjusted
317 to the ambient conditions, which included nighttime samples when the rates were lower. From the T–S
318 diagram (Fig.7), we found that higher photoproduction rates at stations S0701 and S0704 might resulted
319 from the influence of the Kuroshio (see Fig. 1), with enhanced concentrations of NO_2^-. The higher NO
320 production rates measured for stations S0303/S0307 and S0717–S0723 might have been influenced by
321 the South Equatorial and North Equatorial Currents, respectively, but were obviously not associated with
322 enhanced NO_2^- concentrations.
323 If we take the missing 30% of f_{NO} in artificial seawater as the experimental error, then in our study, using
324 the J_{NO} in the artificial seawater, the average $\%f_{NO}$ value in natural water was calculated to be 52% (–
325 30%), indicating that there are other unknown nitrogenous compounds, for example, NO_2^- produced from
326 NO_3^- photolysis (R8) or from other organic matter which could further lead to NO production (Kieber et
327 al., 1999; Benedict et al., 2017; Goldstein and Rabani, 2007; Minero et al., 2007).
328 According to the photoproduction rates and the relevant NO_2^- in Olasehinde et al. (2010), Anifowose
329 and Sakugawa (2017) (Table 1), the photoproduction rates under lower than 0.02 μmol L^{-1} NO_2^- might
330 not be determined in nearshore waters like the Seto Inland Sea.

331 **3.6 Flux densities of NO in the surface layer of the WTNP**

332 **3.6.1 Air–sea flux density of NO**

333 The NO flux densities were computed with (Eq 6):

334 $$F = k_{sea}([NO] - pNO_{air} \times H^{cp}) \quad \text{(Eq 6)}$$

335 $$pNO_{air} = x'NO_{air} \times (p_{ss} - p_w) \quad \text{(Eq 7)}$$

336 here F stands for the flux density (mass $area^{-1}$ $time^{-1}$) across the air–sea interface, k_{sea} is the gas transfer
337 velocity (length $time^{-1}$), [NO] is the measured concentration of NO in the surface seawater (mole $volumn^{-1}$),
338 $x'NO_{air}$ is the mixing ratio of atmosphere NO (dimensionless). And p_{ss} is the barometric pressure
339 while p_w was calculated after Weiss and Price (1980):

$$\ln p_w = 24.4543 - 6745.09/(T + 273.15) - 4.8489 \times \ln (T + 273.15)/100) - 0.000544 \times S) \quad \text{(Eq 8)}$$

H^{cp} is the Henry's law constant which is calculated after Sander (2015) as:

$$H^{cp}(T) = H^{\Theta} \times \exp (-\Delta sol\, H/R \times (1/T - 1/T^{\Theta}) \quad \text{(Eq 9)}$$

where $-\Delta sol \frac{H}{R} = \frac{dlnH}{dln(\frac{1}{T})}$, H^{Θ}, and $-\Delta sol\, H/R$ are tabulated in Sander (2015) ($-\Delta sol\, H/R$=1600 and H^{Θ}=1.9 ×10^{-5} mol m^{-3} pa^{-1}). The reviewed several literatures about NO, H^{Θ} and the values in different literatures were similar (Sander, 2015). In our calculation, the value in the Warneck and Williams (2012) were used.

Then k_{sea} was calculated after (Wanninkhof, 2014) as (Eq 10),

$$k_{sea} = k_w (1 - \gamma_a) \quad \text{(Eq 10)}$$

γ_a is the fraction of the entire gas concentration gradient across the airside boundary layer as a fraction of the entire gradient from the bulk water to the bulk air (dimensionless), k_a is the air side air-sea gas transfer coefficient (length time^{-1}) according to (Mcgillis et al., 2000;Jähne et al., 1987;Sharqawy et al., 2010), for the details of the calculation of k_w and γ_a see Tian et al. (2018).

Since onboard wind speeds were not available, ECMWF reanalysis data sets (ERA-5 hourly data) were applied. We used a value of 10^{-11} (v/v) for atmospheric NO (Law, 2001). The atmosphere pressure was set to 101.325 kPa.

Since the measurements [NO] were not available from the cruise we estimated [NO] by assuming that (1) NO production is mainly resulting from NO_2^- photodegradation and (2) the NO photoproduction R_{NO} as measured in our irradiation experiment is balanced by the NO scavenging rate R_s (3) rates of nitrite photoproduction into NO was proportional to the irradiance flux in order to adjust the rates under simulator light into ambient light at the sampling time (Zafiriou and McFarland, 1981; Olasehinde et al., 2010):

$$R_{NO} \times \frac{I_{ambient}}{I_{simulator}} = [NO] \times R_s, \quad \text{(Eq 11)}$$

where R_s represents the sum of the rate constants for the scavenging compounds reacting with NO times the concentrations of the scavenger compounds, $I_{ambient}$ and $I_{simulator}$ denote the light intensity of the sampling station and the CPS+ simulator (765 W m^{-2}). $I_{ambient}$ was ECMWF reanalysis data sets (ERA-5 hourly data, interpolation method). In the study of Zafiriou et al., (1980) and Anifowose and Sakugawa, (2017), they reviewed the NO lifetime in the different area for the Kurose River (0.05–1.3 s), the Seto Inland sea (1.8–20 s), and the central Equatorial Pacific (40-200 s, 170 °E Equatorial regions),

which showed an increasing trend from river to open sea. It seemed that NO life time in our study area should be most similar to the central Equatorial Pacific. Considering part of our sampling stations were in open sea while some stations were close to continent like New Guinea Island and Japan, average lifetime about 100 s were applied in our study, however the uncertainty was not reported in the literature, but estimated uncertainty about 30% might be appropriate. Tian et al (2018) found that NO concentration in the surface water showed no significant difference with that in the bottom water (average depth: 43 m), so it seems reasonable to estimate the steady state NO concentration with the NO concentration in the mixed layer. Then [NO] was estimated to range from 0 to 292 $\times 10^{-12}$ mol L^{-1} (0 means that sampling time during nighttime), with an average of 49 $\times 10^{-12}$ mol L^{-1}, which was consistent with previous results in central equatorial Pacific (46 $\times 10^{-12}$ mol L^{-1}), while it was lower than near continent seawater like the Seto Inland Sea (up to 120 $\times 10^{-12}$ mol L^{-1}) and the Jiaozhou Bay (157 $\times 10^{-12}$ mol L^{-1}), which might be because of higher nitrite concentration. NO showed lowest concentration in the Kurose River, which might because of less nitrite, and shortest life time might also account for this in river water than in seawater (Anifowose and Sakugawa, 2017).

In Table 1, the resulting flux density of NO for WTNP ranged from 0 to 13.9 $\times 10^{-12}$ mol m^{-2} s^{-1}, with an average of 1.8 $\times 10^{-12}$ mol m^{-2} s^{-1}, which is in good agreement with that in central equatorial Pacific (see Table 1) while it was lower than that in costal seawater such as the Seto Inland Sea or the Jiaozhou Bay, consistent with NO concentration distribution.

3.6.2 Oceanic photoproduction rates of NO

The photoproduction rates from our irradiation experiments were extrapolated to the oceanic photoproduction in the WTNP with the equation from (Bange and Uher, 2005; Uher and Andreae, 1996)

$$R_{ocean} = R_{NO} \times \left(\frac{I_{ocean}(1-exp(-K_D \times MLD))}{I_{ss} \times K_D \times MLD} \right) \quad \text{(Eq 12)}$$

where R_{ocean} and R_{NO} are the photoproduction rates for the ocean mixed layer and seawater irradiation experiments, respectively, see Section 3.5. I_{ocean} and I_{ss} are the average global irradiance at the surface of the ocean mixed layer and the solar simulator used here, K_D is the light attenuation coefficient and MLD is the estimated mixed layer depth at the sampled station.

I_{ocean} was set to 185 W m^{-2}, while I_{ss} was 765 W m^{-2} in our study (Bange and Uher, 2005; Wu et al., 2015). As described above, K_{D-354} was applied to estimate the MLD. In Smyth (2011), K_{D-340} to K_{D-380} derived from 10% residual light level depths ranged from 0.04 m^{-1} to 0.07 m^{-1} for our study area, we used

the average value of 0.05. The MLD was taken as the layer depth where the temperature was 0.2 ℃ lower than the 10 m near–face seawater layer (Montégut, 2004), ranging from 13 – 77 m with an average of 37 m. The resulting average R_{ocean} was about 8.6 ± 4.9 × 10^{-12} mol L^{-1} min^{-1} for the WTNP at the time of our cruise. Besides, the temperature at 20 ℃ in our laboratory experiment would induce about 10% error (Fig. 4e).

The flux induced by NO photoproduction in the WTNP (NO photoproduction rates divide by MLD, average: 13 ×10^{-12} mol m^{-2} s^{-1}) were significantly larger than the NO air–sea flux densities (average: 1.8 ×10^{-12} mol m^{-2} s^{-1}) indicating a further NO loss process in the surface layer.

Conclusion

The results of our irradiation experiments showed that NO photoproduction from NO_2^- in artificial seawater is significantly affected by changes in pH, temperature and salinity. We found increasing NO production rates from dissolved NO_2^- with decreasing pH, increasing temperatures and increasing salinity. In contrast we did not find any correlations of NO photoproduction with pH, salinity, water temperature as well as dissolved NO_2^- in natural surface seawater samples from a cruise to the western tropical North Pacific Ocean (November 2015 – January 2016). We conclude that the trends observed in our irradiation experiments with artificial seawater do not seem to be representative for WTNP because of the complex settings of open ocean environments. Moreover, we conclude that future changes of NO photoproduction due to ongoing environmental changes such as ocean warming and acidification are, therefore, difficult to predict and need to be tested by irradiation experiments of natural seawater samples under varying conditions. The flux induced by NO photoproduction in the WTNP (average: 13 ×10^{-12} mol m^{-2} s^{-1}) were significantly larger than the NO air–sea flux densities (average: 1.8 ×10^{-12} mol m^{-2} s^{-1}) indicating a further NO loss process in the surface layer. This indicates a further NO loss process in the surface layer of the WTNP. In order to decipher and to quantify the NO production and consumption pathways in the oceanic surface layer more comprehensive laboratory and onboard measurements are required.

Author contributions.

YT, GY, CL, HC and PL prepared the original manuscript and designed the experiments; HB made many modifications and gave a lot of suggestions on design of figures and the computing method. All authors contributed to the analysis of the data and discussed the results.

Competing interests.

The authors declare that they have no conflict of interest.

Acknowledgement

We thank the captain and crew of the R/V "Dong Fang Hong 2" for their support and help during the cruise. This research was supported by the National Natural Science Foundation of China (Nos.41676065), the National Key Research and Development Program of China (Grant No. 2016YFA0601301), and the Fundamental Research Funds for the Central Universities (No. 201762032).

References

Anifowose, A. J., Takeda, K., and Sakugawa, H.: Photoformation rate, steady-state concentration and lifetime of nitric oxide radical (NO·) in a eutrophic river in Higashi-Hiroshima, Japan, Chemosphere, 119, 302-309, 2015.

Anifowose, A. J., and Sakugawa, H.: Determination of Daytime Flux of Nitric Oxide Radical (NO·) at an Inland Sea-Atmospheric Boundary in Japan, J. Aquat. Pollut. Toxicol., 1, 1-6, 2017.

Astier, J., Jeandroz, S., and Wendehenne, D.: Nitric oxide synthase in plants: The surprise from algae, Plant Sci., 268, 64-66, 2018.

Bajt, O., Šket, B., and Faganeli, J.: The aqueous photochemical transformation of acrylic acid, Mar. Chem., 58, 255-259, 1997.

Bange, H. W., and Uher, G.: Photochemical production of methane in natural waters: implications for its present and past oceanic source, Chemosphere, 58, 177-183, 2005.

Bange, H. W.: Gaseous Nitrogen Compounds (NO, N_2O, N_2, NH_3) in the Ocean, Elsevier 51–94 pp., 2008.

Benedict, K. B., Mcfall, A. S., and Anastasio, C.: Quantum Yield of Nitrite from the Photolysis of Aqueous Nitrate above 300 nm, Environ. Sci. Technol., 51, 4387-4395, 2017.

Chu, L., and Anastasio, C.: Temperature and wavelength dependence of nitrite photolysis in frozen and aqueous solutions, Environ. Sci. Technol., 41, 3626-3632, 2007.

Clarke, K., Edge, R., Johnson, V., Land, E. J., Navaratnam, S., and Truscott, T. G.: The carbonate radical: its reactivity with oxygen, ammonia, amino acids, and melanins, J. Phys. Chem. A, 112, 10147-10151, 2008.

Fine, R. A., Lukas, R., Bingham, F. M., Warner, M. J., and Gammon, R. H.: The western equatorial Pacific: A water mass crossroads, J. Geophys. Res.: Oceans, 99, 25063-25080, 1994.

Goldstein, S., and Rabani, J.: Mechanism of Nitrite Formation by Nitrate Photolysis in Aqueous Solutions: The Role of Peroxynitrite, Nitrogen Dioxide, and Hydroxyl Radical, J. Am. Chem. Soc., 129, 10597, 2007.

Jähne, B., Heinz, G., and Dietrich, W.: Measurement of the diffusion coefficients of sparingly soluble gases in water, J. Geophys. Res.: Oceans, 92, 10767–10776, 1987.

Joussotdubien, J., and Kadiri, A.: Photosensitized Oxidation of Ammonia by Singlet Oxygen in Aqueous Solution and in Seawater, Nature, 227, 700-701, 1970.

Kieber, D. J., Jiao, J., Kiene, R. P., and Bates, T. S.: Impact of dimethylsulfide photochemistry on methyl sulfur cycling in the Equatorial Pacific Ocean, J. Geophys. Res.: Oceans, 101, 3715-3722, 1996.

Kieber, R. J., Li, A., and Seaton, P. J.: Production of nitrite from the photodegradation of dissolved organic matter in natural waters, Environ. Sci. Technol., 33, 717-723, 1999.

Kuypers, M. M. M., Marchant, H. K., and Kartal, B.: The microbial nitrogen-cycling network, Nat. Rev. Microbiol., 16, 263-276, 2018.

Lantoine, F., Trévin, S., Bedioui, F., and Devynck, J.: Selective and sensitive electrochemical measurement of nitric oxide in aqueous solution: discussion and new results, J. Electroanal. Chem., 392, 85-89, 1995.

Laszlo, B., Alfassi, Z. B., Neta, P., and Huie, R. E.: Kinetics and Mechanism of the Reaction of $\bullet NH_2$ with O_2 in Aqueous Solutions, J. Phys. Chem. A, 102, 8498-8504, 1998.

Law, C. S.: Air–sea transfer: N_2O, NO, CH_4 , CO, Encyclopedia of Ocean Sciences, 137-144, 2001.

Li, P. F., Li, W. S., Liu, C. Y., Zhu, X. C., and Zhang, Q.: The photodecomposition of nitrite in water (in Chinese), Chin. J. Environ. Sci., 30, 1883-1888, 2011.

Li, Y., Mao, Y., Liu, G., Tachiev, G., Roelant, D., Feng, X., and Cai, Y.: Degradation of methylmercury and its effects on mercury distribution and cycling in the Florida Everglades, Environ. Sci. Technol., 44, 6661-6666, 2010.

Liu, C. Y., Feng, W. H., Tian, Y., Yang, G. P., Li, P. F., and Bange, H. W.: Determination of dissolved nitric oxide in coastal waters of the Yellow Sea off Qingdao, Ocean Sci., 13, 623-632, 2017.

Lutterbeck, H. E., and Bange, H. W.: An improved method for the determination of dissolved nitric oxide (NO) in seawater samples, Ocean Sci., 11, 959-981, 2015.

Mack, J., and Bolton, J. R.: Photochemistry of nitrite and nitrate in aqueous solution: a review, J. Photochem. Photobiol., A, 128, 1-13, 1999.

Mcgillis, W. R., Dacey, J. W. H., Frew, N. M., Bock, E. J., and Nelson, R. K.: Water-air flux of dimethylsulfide, J. Geophys. Res.: Oceans, 105, 1187–1193, 2000.

Minero, C., Chiron, S., Falletti, G., Maurino, V., Pelizzetti, E., Ajassa, R., Carlotti, M. E., and Vione, D.: Photochemincal processes involving nitrite in surface water samples, Aquat. Sci., 69, 71-85, 2007.

Montégut, C. D. B.: Mixed layer depth over the global ocean: An examination of profile data and a profile-based climatology, J. Geophys. Res.: Oceans, 109, -, 2004.

Olasehinde, E. F., Takeda, K., and Sakugawa, H.: Development of an analytical method for nitric oxide radical determination in natural waters, Anal. Chem., 81, 6843-6850, 2009.

Olasehinde, E. F., Takeda, K., and Sakugawa, H.: Photochemical Production and Consumption Mechanisms of Nitric Oxide in Seawater, Environ. Sci. Technol., 44, 8403-8408, 2010.

Sander, R.: Compilation of Henry's law constants (version 4.0) for water as solvent, Atmos. Chem. Phys., 14, 29615-30521, 2015.

Schreiber, F., Wunderlin, P., Udert, K. M., and Wells, G. F.: Nitric oxide and nitrous oxide turnover in natural and engineered microbial communities: biological pathways, chemical reactions, and novel technologies, Front. Microbiol., 3, 372, 2012.

Sharqawy, M. H., V, J. H. L., and Zubair, S. M.: Thermophysical properties of seawater: a review of existing correlations and data, Desalin. Water Treat., 16, 354-380, 2010.

Singh, V. K., and Lal, B.: Nitric oxide (NO) stimulates steroidogenesis and folliculogenesis in fish, Reproduction, 153, 133, 2016.

Smyth, T. J.: Penetration of UV irradiance into the global ocean, J. Geophys. Res.: Oceans, 116, 20-32, 2011.

Tian, Y., Xue, C., Liu, C. Y., Yang, G. P., Li, P. F., Feng, W. H., and Bange, H. W.: Nitric oxide (NO) in the Bohai and Yellow Seas, Biogeosciences Discuss.(DOI: 10.5194/bg-2018-446), 2018, 1-25, 2018.

Tugaoen, H. O. N., Herckes, P., Hristovski, K., and Westerhoff, P.: Influence of ultraviolet wavelengths on kinetics and selectivity for N-gases during TiO_2 photocatalytic reduction of nitrate, Appl. Catal., B, 220, 597-606, 2018.

Uher, G., and Andreae, M. O.: The diel cycle of carbonyl sulfide in marine surface waters: Field study results and a simple model, Aquatic Geochemistry, 2, 313-344, 1996.

Wang, B., Dan, L., Chao, W., Wang, Q., Hui, Z., Liu, G., Xia, T., and Zhang, L.: Mechanism of endothelial nitric oxide synthase phosphorylation and activation by tentacle extract from the jellyfish Cyanea capillata, Peerj, 5, e3172, 2017.

Wanninkhof, R.: Relationship between wind speed and gas exchange over the ocean revisited, Limnol. Oceanogr. Methods, 12, 351-362, 2014.

Weiss, R. F., and Price, B. A.: Nitrous oxide solubility in water and seawater, Mar. Chem., 8, 347-359, 1980.

Wu, X., Liu, C. Y., and Li, P. F.: Photochemical transformation of acrylic acid in seawater, Mar. Chem., 170, 29-36, 2015.

Xing, L., Zhang, Z. B., Liu, C. Y., Wu, Z. Z., and Lin, C.: Amperometric Detection of Nitric Oxide with Microsensor in the Medium of Seawater and Its Applications, Sensors, 5, 537-545, 2005.

Xue, C., Liu, C., Yang, G., Zhu, C., and Zhang, H.: Distribution and controlling factors of nitric oxide concentrations in surface seawater of Jiaozhou Bay and adjacent waters (in Chinese), Chin. J. Environ. Sci., 33, 1086-1090, 2012.

Yang, G. P., Ren, C. Y., Lu, X. L., Liu, C. Y., and Ding, H. B.: Distribution, flux, and photoproduction of carbon monoxide in the East China Sea and Yellow Sea in spring, J. Geophys. Res.: Oceans, 116, 1-15, 2011.

Zafiriou, O. C., and True, M. B.: Nitrite photolysis in seawater by sunlight ☆, Mar. Chem., 8, 33-42, 1979.

Zafiriou, O. C., Mcfarland, M., and Bromund, R. H.: Nitric oxide in seawater, Science, 207, 637, 1980.

Zafiriou, O. C., and McFarland, M.: Nitric oxide from nitrite photolysis in the central equatorial Pacific, J. Geophys. Res.: Oceans, 86, 3173–3182, 1981.

Zellner, R., Exner, M., and Herrmann, H.: Absolute OH quantum yields in the laser photolysis of nitrate, nitrite and dissolved H 2 O 2 at 308 and 351 nm in the temperature range 278–353 K, J. Atmos. Chem., 10, 411-425, 1990.

Zhang, Z., Qiu, B., Tian, J., Zhao, W., and Huang, X.: Latitude-dependent finescale turbulent shear generations in the Pacific tropical-extratropical upper ocean, Nat. Commun., 9, 4086, 2018.

Zhao, J., Li, Y., and Wang, F.: Seasonal variation of the surface North Equatorial Countercurrent (NECC) in the western Pacific Ocean, Chin. J. Oceanol. Limnol., 34, 1332-1346, 2016.

Zhu, W. Z., Zhang, J., and Yang, G. P.: Mixing behavior and photobleaching of chromophoric dissolved organic matter in the Changjiang River estuary and the adjacent East China Sea, Estuarine, Coastal Shelf Sci., 2017.

Figure Captions

Fig. 1. Locations of the sampling stations in the western tropical North Pacific Ocean. The acronyms NGCC, SEC, NECC, NEC, and STCC stand for New Guinea Coastal Current, South Equatorial Current, North Equatorial Counter Current, North Equatorial Current, and Subtropical Counter Current, respectively.

Fig. 2. Changes of NO concentrations with initial DAF–2 concentration of 0, 0.7, 1.4, 2.1, 2.8, 3.5 and 4.2 μmol L^{-1} after irradiation time of 2 h (a) and changes of different NO concentrations with storage time monitored at about 2 h time intervals (b).

Fig. 3. Photoproduction rates of NO with 0.5, 2, and 5.0 μmol L^{-1} NO_2^- (a) and the calculated J_{NO} values in Milli–Q water and artificial seawater (b), symbols in red represented for the artificial seawater samples and in black for Milli–Q water.

Fig. 4. NO concentration changes with irradiation time at different pH, salinity, temperature and waveband conditions (a, c, e, g for 0.5 μmol L^{-1} NO_2^- and b, d, f, h for 5.0 μmol L^{-1} NO_2^-).

Fig. 5. Changes of NO photoproduction rates with irradiation time at different pH, salinity, temperature and waveband conditions (a, c, e, g for 0.5 μmol L^{-1} NO_2^- and b, d, f, h for 5.0 μmol L^{-1} NO_2^-).

Fig. 6. Seawater temperature, salinity, concentrations of NO_2^-, NO_3^-, NH_4^+, and photoproduction rates of NO (R_{NO}) in the western tropical North Pacific Ocean. (a: W/E transect; b: N/S transect)

Fig. 7. The potential temperature–salinity (T–S) diagram with NO photoproduction rates indicated in the color bar. Water mass characteristics of surface currents shown in Figure 1 are indicated. The acronyms NGCC, SEC, NECC, NEC, and STCC stand for New Guinea Coastal Current, South Equatorial Current, North Equatorial Counter Current, North Equatorial Current, and Subtropical Counter Current, respectively.

573

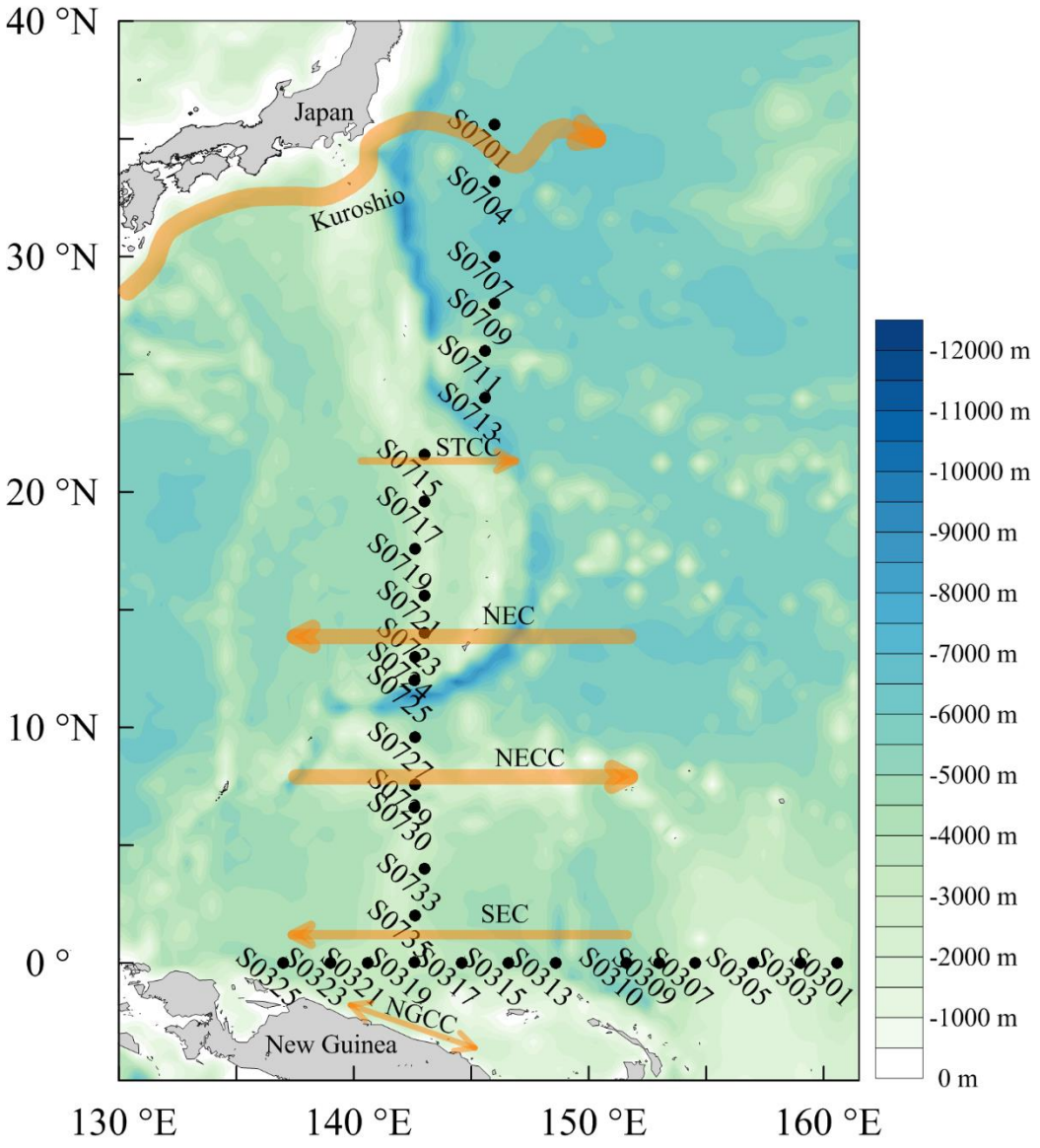

574

575

576 **Fig. 1.** Locations of the sampling stations in the western tropical North Pacific Ocean. The
577 acronyms NGCC, SEC, NECC, NEC, and STCC stand for New Guinea Coastal Current, South
578 Equatorial Current, North Equatorial Counter Current, North Equatorial Current, and Subtropical
579 Counter Current, respectively.

580

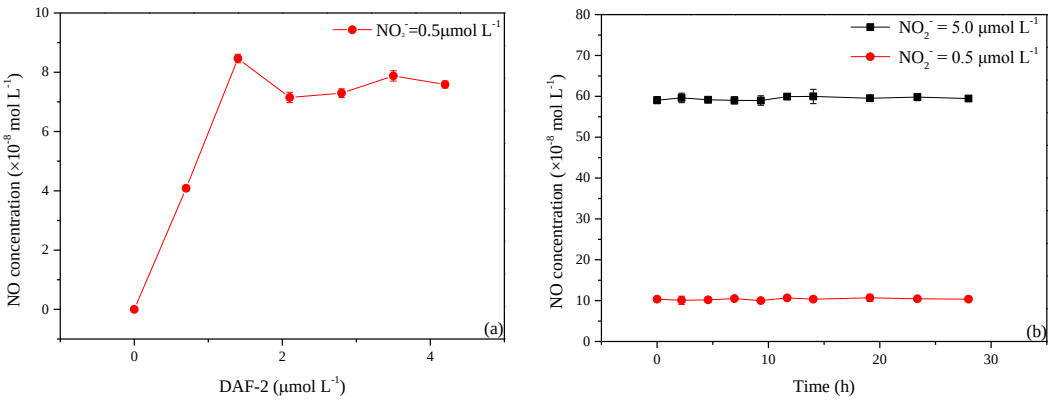

581

582 **Fig. 2.** Changes of NO concentrations with initial DAF–2 concentration of 0, 0.7, 1.4, 2.1, 2.8, 3.5 and

583 4.2 μmol L^{-1} after irradiation time of 2 h (a) and changes of different NO concentrations with storage

584 time monitored at about 2 h time intervals (b).

585

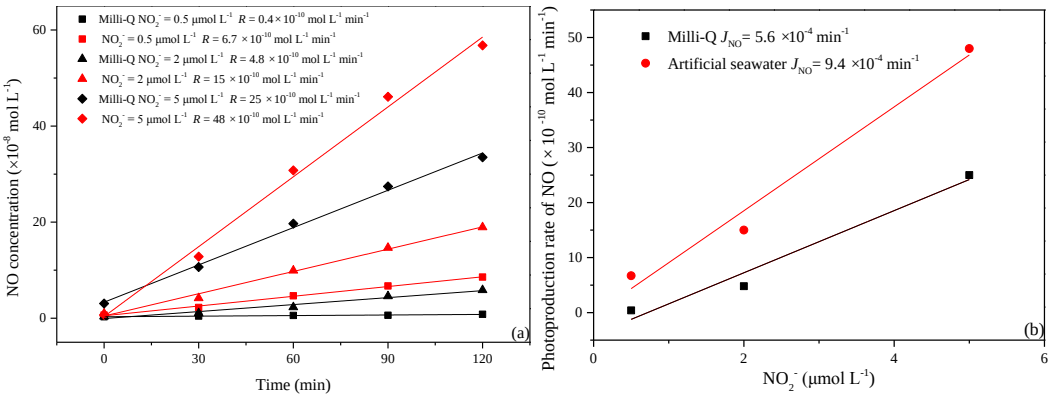

Fig. 3. Photoproduction rates of NO with 0.5, 2, and 5.0 µmol L^{-1} NO_2^- (a) and the calculated J_{NO} values in Milli–Q water and artificial seawater (b), symbols in red represented for the artificial seawater samples and in black for Milli–Q water.

592

593

594

595

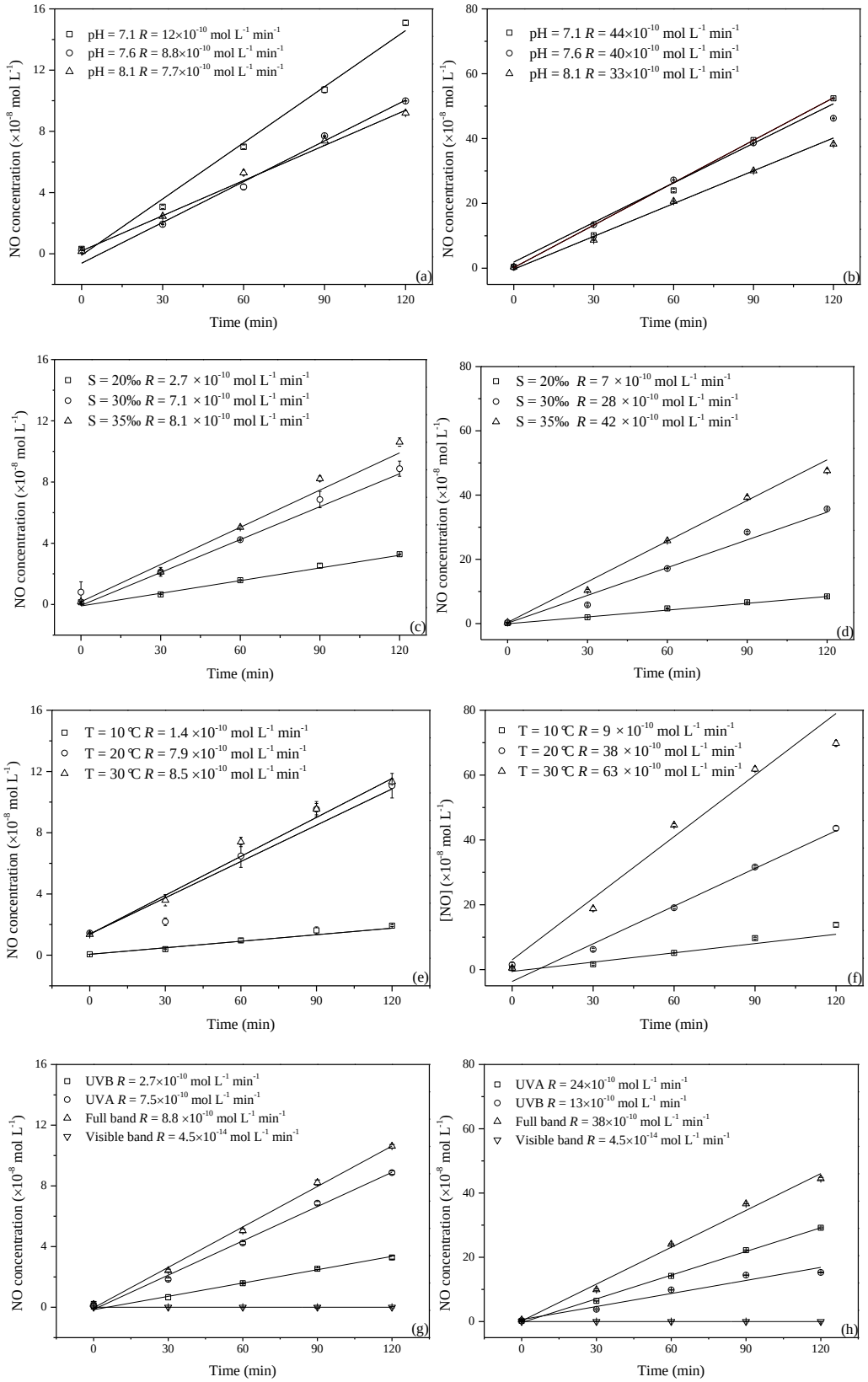

596 **Fig. 4.** NO concentration changes with irradiation time at different pH, salinity, temperature and

597 waveband conditions (a, c, e, g for 0.5 μmol L^{-1} NO_2^- and b, d, f, h for 5.0 μmol L^{-1} NO_2^-).

598

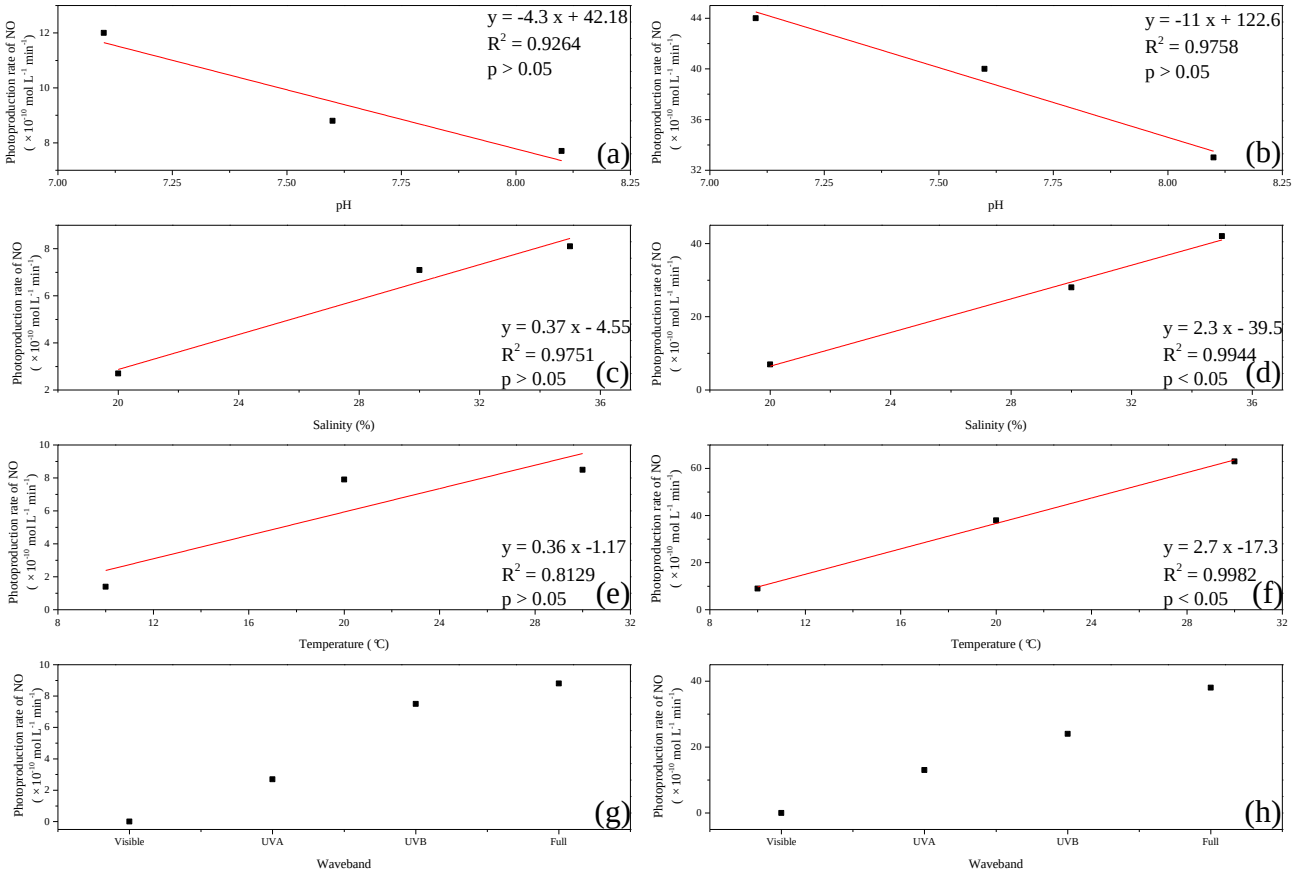

Fig. 5. Changes of NO photoproduction rates with irradiation time at different pH, salinity, temperature and waveband conditions (a, c, e, g for 0.5 μmol L^{-1} NO_2^- and b, d, f, h for 5.0 μmol L^{-1} NO_2^-).

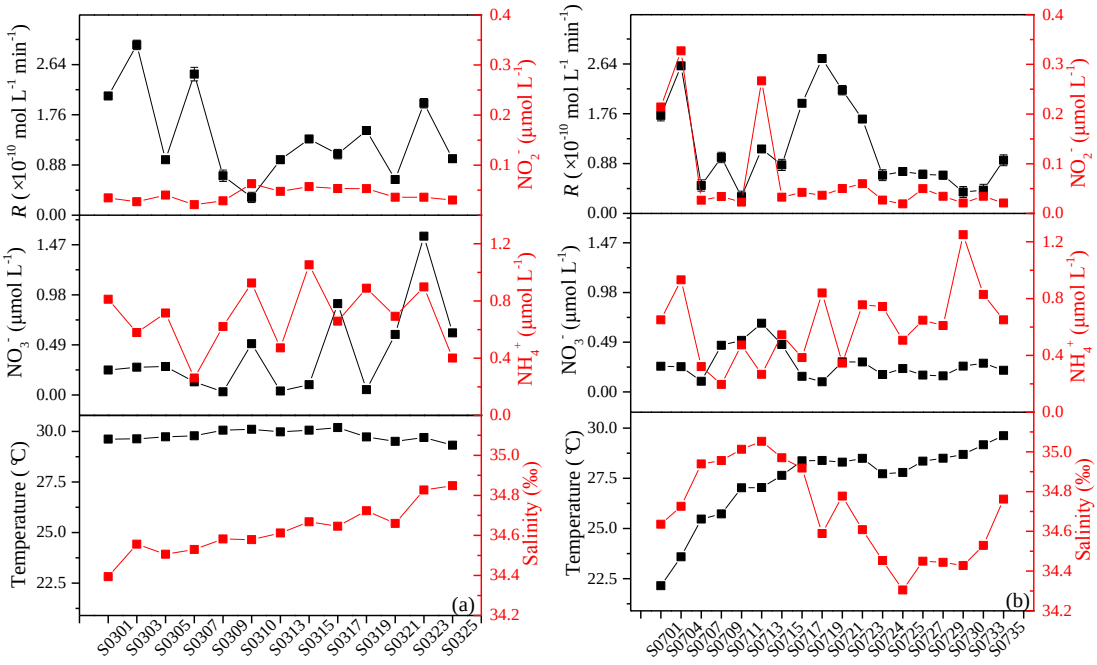

Fig. 6. Seawater temperature, salinity, concentrations of NO_2^-, NO_3^-, NH_4^+, and photoproduction rates of NO (R_{NO}) in the western tropical North Pacific Ocean (a: W/E transect; b: N/S transect.).

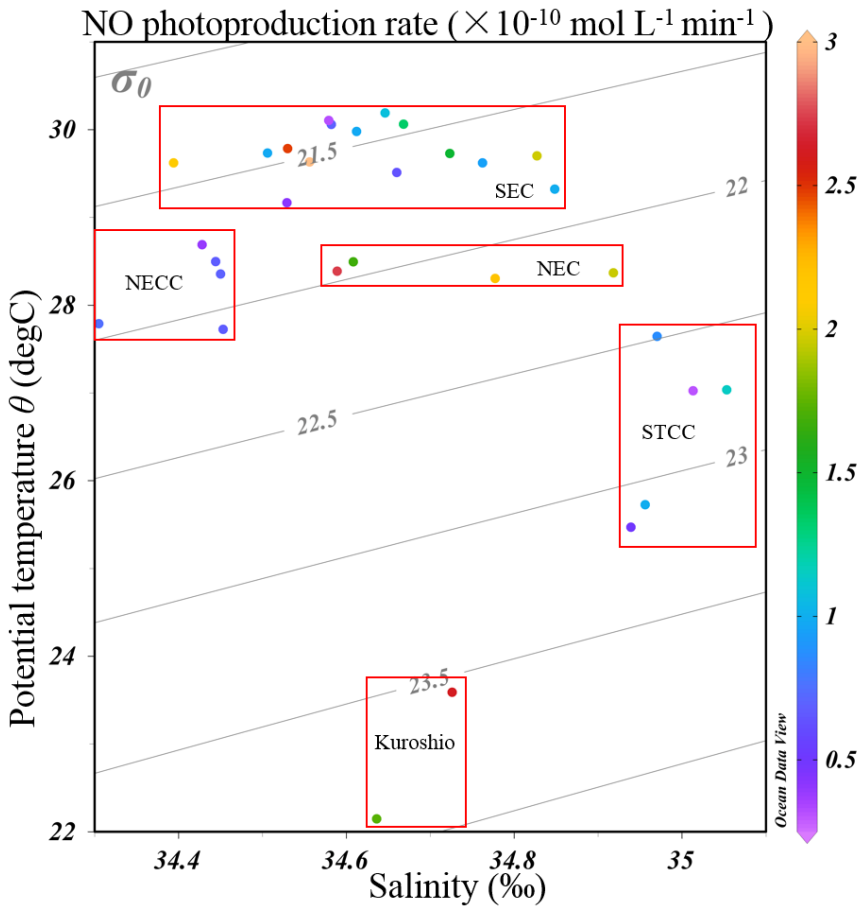

608

609 **Fig. 7.** The potential temperature–salinity (T–S) diagram with NO photoproduction rates indicated in

610 the color bar. Water mass characteristics of the surface currents shown in Figure 1 are indicated. The

611 acronyms NGCC, SEC, NECC, NEC, and STCC stand for New Guinea Coastal Current, South

612 Equatorial Current, North Equatorial Counter Current, North Equatorial Current, and Subtropical

613 Counter Current, respectively.

614

Table Captions

Table 1 Photoproduction rates (R), average NO concentrations and average flux densities of NO in different regions.

Table 2 The ratios of photoproduction rates ($R5.0/R0.5$) in the different irradiation experiments.

620 **Table 1** Photoproduction rates (*R*), average NO concentrations, NO_2^- concentrations and average flux

621 densities of NO in different regions.

Regions	*R* (mol L^{-1} s^{-1})	NO (mol L^{-1})	NO_2^- μmol L^{-1}	Flux (mol m^{-2} s^{-1})	Sampling date	References
Seto Inland Sea, Japan	$8.7–38.8\times10^{-12}$	120×10^{-12}	0.5-2	3.55×10^{-12}	October 5–9, 2009	Olasehinde et al., 2010
Seto Inland Sea, Japan	$1.4\text{-}9.17\times10^{-12}$	$3\text{-}41\times10^{-12}$	0-0.4	0.22×10^{-12}	September, 2013 and June, 2014	Anifowose and Sakugawa, 2017
Kurose River, Japan	$9.4–300\times10^{-12}$	–	-	–	–	Olasehinde et al., 2009
Kurose River (K1 station), Japan	4×10^{-12}	1.6×10^{-12}	0.06	–	Monthly, 2013	Anifowose et al., 2015
Jiaozhou Bay	–	157×10^{-12}	-	7.2×10^{-12}	June, July and August, 2010	Tian et al., 2016
Jiaozhou Bay and its adjacent waters	–	$(160\pm130)\times10^{-12}$	-	10.9×10^{-12}	March 8–9, 2011	Xue et al., 2011
Coastal water off Qingdao	1.52×10^{-12}	260×10^{-12}	0.75	-	November, 2009	Liu et al., 2017
Central equatorial Pacific	$> 10^{-12}$	46×10^{-12}	0.2	2.2×10^{-12}	R/V Knorr 73/7	Zafiriou and Mcfarland., 1981
The northwest Pacific Ocean	$0.5\pm0.2\times10^{-12}$	49×10^{-12}	0.06	1.8×10^{-12}	November 15, 2015 to January 26, 2016	This study

622

623 **Table 2** The ratios of photoproduction rates (*R*5.0/*R*0.5) in the different irradiation experiments.

	R ($\times 10^{-10}$ mol L^{-1} min^{-1})		Ratio
	0.5 μM	5.0 μM	
pH=7.1	12	44	3.7
pH=7.6	8.8	40	4.5
pH=8.1	7.7	33	4.3
T=10 ℃	1.4	9.0	6.4
T=20 ℃	7.9	38	4.8
T=30 ℃	8.5	63	7.4
S=20	2.7	7.0	2.6
S=30	7.1	28	3.9
S=35	8.1	42	5.2

624